Journal of Molecular Liquids 367 (2022) 120480

Contents lists available at ScienceDirect

Journal of Molecular Liquids

journal homepage: www.elsevier.com/locate/molliq

Diffusivities of linear unsaturated ketones and aldehydes in compressed liquid ethanol

Bruno Zêzere [a], Simon Buchgeister [b], Sofia Faria [a], Inês Portugal [a], José R. B. Gomes [a,*], Carlos M. Silva [a,*]

[a] CICECO – Aveiro Institute of Materials, Department of Chemistry, University of Aveiro, Campus Universitário de Santiago, 3810-193 Aveiro, Portugal
[b] Faculty of Biochemical and Chemical Engineering, TU Dortmund University, Emil-Figge-Straße, 70, D-44227 Dortmund, Germany

ARTICLE INFO

Article history:
Received 4 August 2022
Revised 20 September 2022
Accepted 24 September 2022
Available online 30 September 2022

Keywords:
Aldehydes
Chromatographic peak broadening technique
Diffusion coefficients
Experimental measurement
Ketones
Machine Learning
Modelling

ABSTRACT

For the accurate design, optimization and simulation of chemical processes limited by mass transfer kinetics it is important the knowledge of transport properties, namely, diffusion coefficients, D_{12}. In this work, the D_{12} values of six unsaturated linear ketones (*i.e.*, propanone, butanone, propan-2-one, propan-3-one, hexan-2-one and hexan-3-one) and three unsaturated linear aldehydes (*i.e.*, butanal, pentanal and hexanal) in (compressed) liquid ethanol were measured at temperatures from 303.15 K to 333.15 K and pressures up to 150 bar. The D_{12} values of ketones are in the range of 1.28×10^{-5} – 2.89×10^{-5} cm^2 s^{-1} and of the aldehydes are between 1.39×10^{-5} and 2.68×10^{-5} cm^2 s^{-1}. The general trends of D_{12} regarding temperature, pressure, Stokes-Einstein coordinate, and free volume are presented and discussed. The diffusivities of the various ketones position isomers and aldehyde/ketone isomers were statistically compared, being possible to conclude that the former ones exhibit indistinguishable diffusivities while different values appear for aldehydes/ketones isomers. Finally, five models and a machine learning algorithm from the literature were tested to predict/correlate the new data. It is suggested that the TLSM model should be the preferred approach for D_{12} prediction of linear unsaturated aldehydes and ketones in liquid compressed ethanol.

1. Introduction

Cussler [1] pointed out that "diffusion in liquids is important because it is slow" and this is the major motivation to investigate the behavior of solutes in solutions. In fact, the diffusivity of solutes is a limiting rate step in various processes occurring in dense fluids, *e.g.*, reaction rates in chemistry, surface corrosion processes in metallurgy, and extractions using liquid or supercritical solvents [1]. Hence, knowledge about diffusion behavior and diffusion coefficients data are of great importance for practical applications. However, since their experimental measurement for all real mixtures of interest is impossible, the existence of accurate predictive and correlation models is essential for their calculation in binary and multicomponent systems. For this, the accurate knowledge of tracer diffusivities (D_{12}) is required to develop and validate such models, and also to estimate multicomponent diffusivities using the empirical mixing rule of Vignes [2] or the Maxwell-Stefan approach [3,4].

Regarding D_{12}, the data available in the literature are scarce specially concerning polar solvents. Accordingly, in this work, the diffusion coefficients of ketones and aldehydes in compressed liquid ethanol were experimentally determined by the chromatographic peak broadening technique [5–8].

Aldehydes are characterized by the presence of a carbonyl group bonded to one carbon and one hydrogen atom, and are building blocks widely used in organic synthesis [9]. Aldehydes may occur in food as natural constituents, *e.g.* pentanal in red wine and butanal in wheaten bread [10], hexanal in oranges [10,11], or as artificially added flavoring ingredients [10]. Some aldehydes are responsible for very pleasant odors, like benzaldehyde in almonds [12], while others are responsible for unpleasant odors such as the fishery odor of boiled crab meatballs caused by a mixture of pentanal, hexanal, heptanal and decanal [13]. More particular applications of aldehydes include hexanal usage to extend shelf life and retain fruit original color [14–16], and butanal usage in the manufacture of synthetic resins, plasticizers, pharmaceuticals, agrochemicals, antioxidants and perfumery [17].

Analogously to aldehydes, ketones are also characterized by the existence of a carbonyl group but now binding to carbons of two radicals. In general, ketones are more stable than aldehydes [12]. Ketones are used as reactants for the synthesis of pharmaceuticals,

* Corresponding authors.
E-mail addresses: jrgomes@ua.pt (J. R. B. Gomes), carlos.manuel@ua.pt (C. M. Silva).

https://doi.org/10.1016/j.molliq.2022.120480
0167-7322/

Nomenclature

A_{peak}	Area of the peak
ARD	Average relative deviation
AARD	Average absolute relative deviation
B_{12}	Adjustable parameter of Rice and Gray correlation
B_{DHB}	Characteristic constant of the solvent–solute pair from the DHB correlation
$\bar{C}$	Average radial solute concentration
D	Dispersion coefficient
D_{12}	Tracer diffusion coefficient
De	Dean number
DHB	Dymond-Hildebrand-Batchinski
F_{12}	Hard sphere correction factor of D_{12}
$g(\sigma_{eff,12})$	Radial distribution function at contact
L	Length of the column
LJ	Lennard-Jones
m	Quantity of solute injected
m_{12}	Reduced mass of the system
Abs_{max}	Peak maximum absorption
M_i	Molecular weight of the component i
M_{mix}	Weighted average of the solvent mixture
NAI	Ratio between the peak maximum absorbance and its area
N_{av}	Avogadro number
NDP	Number of data points
k_{12}	Binary interaction parameter of the Rice and Gray correlation
$k_{12,d}$	Binary interaction parameter of the $TLSM_d$ model
k_B	Boltzmann constant (1.380649×10^{-23} J K^{-1})
P_c	Critical pressure
Pe_x	Longitudinal Peclet number
R_0	Inner column radius
R_g	Universal gas constant (8.3144 J mol^{-1} K^{-1})
S_{10}	Symmetry factor at 10 % of peak high
Sc	Schmidt number
t	Time
T	Absolute temperature
T_c	Critical temperature
T^*_{12}	Reduced binary absolute temperature
TLSM	Tracer Liu-Silva-Macedo
$\bar{u}$	Mean fluid velocity
$V^{TC}_{bp,i}$	Molar volume at normal boiling point estimated by the Tyn-Calus relation for component i
V_c	Critical molar volume
V_D	Minimum volume required for diffusion from the DHB correlation
V_i	Molar volume of component i

Greek letters

ε	Root mean square error
$\varepsilon_{LJ,i}/k_B$	Lennard Jones energy of the component i
λ	Wavelength
μ_i	Viscosity of compound i
ρ_1	Density of component i
$\rho_{n,i}$	Number density of component i
ρ^*_i	Reduced number density of component i
$\sigma_{LJ,i}$	Lennard-Jones diameter of component i
$\sigma_{eff,i}$	Effective hard sphere diameter of component i
ϕ_i	Association factor of the component i

Subscripts

1	Solvent
2	Solute
12	Solute-solvent pair
c	Critical property
r	Reduced property (using critical constants)

Superscripts

calc	Calculated
exp	Experimental
*	Reduced property (using LJ constants)

dyes, odorants, pesticides, paint and varnish removers or to produce ketone resins in the plastic industry [18]. Besides, ketones are good solvents for paints, cellulose ethers, nitro-cellulose among others [19]. Butanone is one of the most produced industrial chemical compounds and is mainly used as solvent [20].

In this work the D_{12} of six linear unsaturated ketones (propanone, butanone, pentan-2-one, pentan-3-one, hexan-2-one, hexan-3-one) and three linear unsaturated aldehydes (butanal, pentanal and hexanal) were experimentally measured in liquid ethanol by the Chromatographic Peak Broadening (CPB) technique at temperatures between 303.15 K and 333.15 K and pressures between 1 bar and 150 bar [5–8]. Even though aldehydes and ketones are two largely studied chemical families, their diffusion in polar solvents is still largely understudied. In fact, to the best of our knowledge, D_{12} of the present targeted compounds in polar solvents are only available for acetone in chlorotrifluoromethane [21] and water [22]. The remaining literature data refer to D_{12} in weakly polar solvents, namely, acetone in cyclohexane, *n*-dodecane, *n*-hexane and CO_2 [23–28], and butanone, pentan-2-one and pentan-3-one in CO_2 [26,29–31]. As for the target aldehydes, no D_{12} values were found in the literature.

Besides the new experimental data, this work also assesses five equations to model the D_{12} points, namely, the predictive Wilke-Chang (WC) [32,33] and Tracer Liu-Silva-Macedo (TLSM) [34–36] equations, and the correlations of $TLSM_d$ [34–36], Dymond-Hildebrand-Batschinski (DHB) [37–39] and Rice and Gray [40] Furthermore, the predictive computational approach based on a gradient boosted machine learning algorithm proposed by Aniceto *et al.* [41] is also included.

Finally, one may consider these measurements of particular relevance for the development and/or improvement of predictive models, and to enhance the understanding of transport phenomena of compounds with carbonyl functional group. Moreover, the present findings can be further applied to more complex aldehydes and ketones.

2. Theoretical background

2.1. Chromatographic peak broadening technique

Based on the fundamental work developed by Taylor [5–7] and Aris [8], the CPB technique has been widely employed to measure diffusion coefficients at infinite dilution [42,43]. The CPB method is based on the injection of a solute impulse into a laminar flow solvent stream inside a capillary tube. The solute will broaden due to the combined effect of molecular diffusion and convection along the radial direction and longitudinal axis, respectively, and, if an endless tube is involved, a parabolic symmetric peak is obtained

at column outlet [44]. The average radial concentration ($\bar{C}$) profile at column exit, $z = L$, is described by [45]:

$$\bar{C}(L,t) = \left(\frac{m}{\pi {R_0}^2}\right)\frac{\bar{u}}{\sqrt{4\pi D t}}\exp\left[-\frac{\left(L-\bar{u}\,t\right)^2}{4Dt}\right] \quad (1)$$

where m is the quantity of solute injected, R_0 the inner radius of the column, $\bar{u}$ is the mean fluid velocity, t is time, L is the column length, and D is the dispersion coefficient described by:

$$D = D_{12} + \frac{R_0^2 \bar{u}^2}{48 D_{12}} \quad (2)$$

Equation (1) can be fitted to the experimental solute concentration profile by minimizing the root mean square error defined as [26,45]:

$$\varepsilon = \left(\frac{\int_{t1}^{t2}\left(C^{\exp}(L,t) - \bar{C}(L,t)\right)^2 dt}{\int_{t1}^{t2}\left(C^{\exp}(L,t)\right)^2 dt}\right)^{1/2} \quad (3)$$

where t_1 and t_2 are the times at 10 % of the peak height, with $t_1 < t_2$.

The measured peaks quality should be evaluated by a series of conditions described in the literature [26,45–49]. First, the concentration profile should be gaussian shaped, which is true if:

$$\frac{D}{\bar{u}\,L} < 0.01 \quad (4)$$

Axial dispersion should be negligible, which requires large longitudinal Peclet numbers (Pe_x). Perturbations due to temperature and/or pressure changes must be negligible, which is fulfilled if:

$$\frac{\bar{u}\,L}{D} > 1000 \quad (5)$$

Since long capillary columns are required, usually they are coiled inside a thermostatic oven causing a secondary circular flow, whose effect on the diffusivity measurement can be neglected if:

$$De\,Sc^{0.5} < 10 \quad (6)$$

where De is the Dean number and Sc the Schmidt number. Finally, ε should be ideally below 1 %, but acceptable if under 3 % and if the symmetry factor at 10 % of peak high (S_{10}) is lower than 1.3.

2.2. Modelling

Distinct modelling approaches were applied to the experimental data, namely a predictive machine learning algorithm and five classical equations from the most relevant theories available in the literature: Wilke-Chang (WC), from hydrodynamic theory; Dymond-Hildebrand-Batschinski (DHB) and Tracer Liu-Silva-Macedo (TLSM and $TLSM_d$), from free-volume theory; and the model of Zêzere *et al.* [40], from Rice and Gray approach. For optimization and evaluation of the tested models, the absolute average relative deviation (AARD) was employed:

$$\mathrm{AARD}(\%) = \frac{100}{NDP}\sum_{i=1}^{NDP}\left|\frac{D_{12}^{\mathrm{calc}} - D_{12}^{\exp}}{D_{12}^{\exp}}\right|_i \quad (7)$$

where D_{12}^{calc} is the calculated diffusion coefficient, $D_{12}^{\exp}$ is the experimental value, and NDP the number of data points. The tested models are briefly described in the following.

2.2.1. Wilke-Chang (WC) equation

The Wike-Chang (WC) expression is a hydrodynamic equation based on an empirical modification of the Stokes-Einstein relationship. It is described by [32,33]:

$$D_{12} = \frac{7.4\times10^{-8}(\phi_1 M_1)^{1/2} T}{\mu_1 \left(V_{\mathrm{bp},2}^{\mathrm{TC}}\right)^{0.6}} \quad (8)$$

where ϕ is the association factor of the solvent ($\phi = 1.5$ for ethanol), M_1 is the molecular weight of the solvent, T is the absolute temperature, μ_1 is the viscosity of the solvent, and $V_{\mathrm{bp},2}^{\mathrm{TC}}$ is the solute molar volume at normal boiling point estimated, in this study, by the Tyn-Calus relation [50].

2.2.2. Dymond-Hildebrand-Batschinski (DHB) equation

The Dymond-Hildebrand-Batschinski (DHB) 2-parameter correlation based of free-volume theory was originally proposed to describe non-polar systems with negligible attractive forces at moderate densities, though good results are achieved in almost all [36,51] cases. The corresponding two fitting parameters are the minimum molar volume required for diffusion (V_D) and a characteristic parameter of the solvent–solute pair (B_{DHB}) [37–39]. The equation is given by:

$$D_{12} = B_{DHB}\sqrt{T}(V_1 - V_D) \quad (9)$$

where V_1 is the molar volume of the solvent.

2.2.3. Tracer Liu-Silva-Macedo (TLSM and $TLSM_d$) models

The Tracer Liu-Silva-Macedo is a hybrid free volume model that combines both attractive and repulsive interactions. [34–36]. The main equation of the model is:

$$D_{12} = \frac{21.16}{\rho_{n,1}\sigma_{\mathrm{eff},12}^2}\left(\frac{1000 R_g T}{M_{12}}\right)^{1/2}\exp\left(-\frac{0.75\rho_{n,1}^*}{1.2588-\rho_{n,1}^*} - \frac{0.27862}{T_{12}^*}\right) \quad (10)$$

where $\rho_{n,1}$ is the number density of the solvent, $\rho_{n,1}^*$ is the reduced solvent density, $\sigma_{\mathrm{eff},12}$ is the binary effective diameter, M_{12} the reduced molecular weight, T_{12}^* is the reduced binary temperature, and R_g is the universal gas constant (8.3144 J mol^{-1} K^{-1}). The remaining equations required for the calculation of D_{12} can be found elsewhere [36].

As for the $TLSM_d$ 1-parameter correlation, it is similar to TLSM but a binary interaction parameter ($k_{12,d}$) is introduced into the Lennard-Jones (LJ) diameter combining rule:

$$\sigma_{LJ,12} = (1 - k_{12,d})\frac{\sigma_{LJ,1} + \sigma_{LJ,2}}{2} \quad (11)$$

2.2.4. Rice and Gray (RG) correlation

The two-parameter Rice and Gray (RG) improved correlation of dense systems was proposed by Zêzere *et al.* [40]. The main equation is:

$$D_{12} = \frac{k_B T}{\frac{8}{3}\rho_{n,1}\sigma_{\mathrm{eff},12}^2\sqrt{2\pi m_{12} k_B T}\left[\frac{g(\sigma_{\mathrm{eff},12})}{F_{12}} + \frac{B_{12}}{T_{12}^{*1.5}}\right]} \quad (12)$$

where m_{12} is the reduced mass of the system, $g(\sigma_{\mathrm{eff},12})$ is the radial distribution function at contact, F_{12} is the hard sphere correction factor, and B_{12} is an adjustable parameter that englobes the Stockmayer potential. The second adjustable parameter, similarly to the $TLSM_d$ correlation, is a binary interaction parameter (k_{12}) introduced into the LJ diameter combination rule. The remaining model equations can be found in the literature [40].

2.2.5. Machine learning (ML-GB Polar) model

A computational approach proposed by Aniceto *et al.* [41] based on a gradient boosted (GB) machine learning (ML) algorithm was tested, denominated ML-GB Polar. The trained polar diffusivity

model uses several different descriptors, as, for example, temperature, solvent viscosity, solute molar mass, solute critical pressure, solvent molar mass, and the Lennard-Jones energy constant of solvent to predict diffusivity of systems.

3. Materials and methods

3.1. Chemicals

Propanone (C_3H_6O, CAS number 67-64-1, with purity ≥ 99.8 wt.%) and butanone (C_4H_8O, CAS number 78-93-3, with purity ≥ 99.7 wt.%) were purchased from VWR Chemicals; Butanal (C_4H_8O, CAS number 123-72-8, with purity ≥ 99.6 wt.%), pentanal ($C_5H_{10}O$, CAS number 110-62-3, with purity ≥ 97 wt.%), hexanal ($C_6H_{12}O$, CAS number 66-25-1, with purity ≥ 98 wt.%) and pentan-2-one ($C_5H_{10}O$, CAS number 107-87-9, with purity ≥ 99.5 wt.%) were purchased from Sigma Aldrich; pentan-3-one ($C_5H_{10}O$, CAS number 96-22-0, with purity ≥ 99.8 wt.%) was purchased from LGC; hexan-2-one ($C_6H_{12}O$, CAS number 589-38-8, with purity ≥ 98.0 wt.%) and hexan-3-one ($C_6H_{12}O$, CAS number 589-38-8, with purity ≥ 97.5 wt.%) were purchased from Supelco; Ethanol (C_2H_6O, CAS number 67-17-5, with purity ≥ 99.9 wt.%) was purchased from Carlo Erba. All chemicals were used without further purification and stored under the supplier recommend conditions.

3.2. Experimental conditions and equipment

The experiments were carried out following the CPB method, using the experimental setup described by Zêzere *et al.* [52]. Briefly the experimental system is pressurized and a continuous solvent flow is generated by the syringe pump Teledyne ISCO model 100 MD. The reservoir of the pump is filled with ethanol and compressed up to the constant operating pressure, at room temperature. For solvent preheating, a stainless-steel column placed inside the LSIS-B2V/IC 22 oven (Venticell, MMM Group) is used. After tempering, the solvent is feed into a coiled open capillary column (PEEK tubing, with R = 0.261 mm, L = 11.016 m and R_c = 0.15 m) also placed in the oven, whose temperature was set at 303.15, 318.15 and 333.15 K. The column is connected to an UV–Vis detector (Azura DAD 2.1 L, Knauer) to analyze the outlet stream with a recording rate of 1 s at a broad wavelength spectrum. At the end of the system, a back-pressure regulator (Jasco) controls the column pressure, which was set to 1, 75 and 150 bar. After at least 1–2 h of stabilization after changing conditions or after startup of the system, the tracer is injected as an impulse signal. Therefore 0.1 μL of solute is injected by changing the flow path in the injection valve.

4. Results and discussion

The first part of the section focuses the selection of the best wavelength for the measurement and the assessment of the CPB method conditions. Then, the D_{12} experimental data of the aldehydes and ketones are presented and discussed. Finally, the modelling results are disclosed.

4.1. Wavelength study

To determine an accurate wavelength for the UV–Vis detection of the solute at column outlet, a wavelength study was firstly performed for each compound. For this purpose, scans over a spectrum of absorption of the tracer substance were performed between 230 nm and 300 nm for ketones and between 240 nm and 330 nm for aldehydes. The D_{12} value, the ratio between the peak maximum absorbance and its area (*NAI*), root mean square error (ε), and the reproducibility (standard deviation) were compared for the different wavelengths. Ideally, the optimum wavelength should be the one with the lowest ε, the highest reproducibility between different replicas, and that for which a small deviation from the set value does not affect D_{12}. The chosen wavelength for the chromatograms recording was not changed for the different P and T conditions since it was observed that the quality of the results was not influenced as shown in Fig. A.1 for the case of propanone in ethanol. The results for the remaining systems are omitted because similar conclusions were obtained.

As evidenced in Fig. A.1, the ε values go through a minimum and do not vary significantly for most of the analyzed wavelengths. At the edges of the preselected spectrum the fitting error increases and the variability of the measured D_{12} also increases. After carrying out the analyses, the wavelengths selected were: 260 nm for propanone, 270 nm for the remaining ketones, and 284 nm for the aldehydes.

4.2. CPB applicability

The conditions mentioned in section 2.1 were investigated and the applicability of the CPB method ensured: (i) $\bar{u}$ between 0.98 and 1.17 cm s^{-1}; (ii) Re between 4.25 and 7.83; (iii) longitudinal Peclet number, Pe_x, between 4.22×10^7 and 9.52×10^7; (iv) $Sc\sqrt{De} < 8$; (v) $D/\bar{u}L < 0.01$; (vi) $D/\bar{u}L > 1000$ (vii) ε with a maximum of 1.43 %; (viii) S_{10} with a maximum of 1.11. The set-volume flow rate of the syringe pump was double checked by volumetric and gravimetric measurement. Table 1 shows the density and viscosity of ethanol at the various temperature and pressure conditions. The density was calculated by the Tait [53] and the Eykman [54,55] equations, while Mamedov equation [56] was used for viscosity.

4.3. Experimental results

The diffusion coefficient values of all studied compounds are presented in Table 1 along with their standard deviations calculated with four to six replicas (only results with a fitting error ε smaller than 3 % and S_{10} under 1.3 were included), and the solvent (ethanol) density and viscosity.

4.3.1. D_{12} trends with temperature and pressure

The diffusivity of the ketones and aldehydes follows the expected general trends as previously verified for other compounds in dense solvent studies [42,43,52]. First, it can be observed that for any solute the diffusion increases with temperature, which can be attributed to the increasing internal energy of the system that subsequently facilitates solute movement. Second, increasing pressure decreases the D_{12} values, because as the solvent molecules become more packed the free volume for diffusion is reduced and the energy needed by the solute molecules to escape from the force field of the solvent increases [57–59].

4.3.2. D_{12} trends with solute size

The comparison of the D_{12} values between the different ketones reveals that longer hydrocarbon chains (higher number of carbons) have lower D_{12} values as evidenced in Fig. 1 (a). This can be directly explained by the Stokes-Einstein relation, which states that diffusion should decrease with increasing molecule size, thus smaller solutes diffuse faster [33]. The aldehydes exhibit the same behavior as ketones, as illustrated in Fig. 1 (b). This trend was also identified experimentally and by molecular dynamics studies for ketones in SC-CO_2 [26,60].

Table 1
Diffusivities (D_{12}) of the studied ketones and aldehydes in liquid ethanol at the respective T and P, along with ethanol density (ρ_1) and viscosity (μ_1).

T (K)	P (bar)	Ethanol		Propanone	Butanone	Butanal	Pentan-2-one	Pentan-3-one	Pentanal	Hexan-2-one	Hexan-3-one	Hexanal
		ρ_1[†] (g cm^{-3})	μ_1[*] (cP)	$D_{12} \pm \Delta D_{12}$[††] (10^{-5} cm^{2}s^{-1})								
303.15	1	0.7816	0.9645	1.94 ± 0.03	1.75 ± 0.03	1.94 ± 0.07	1.57 ± 0.02	1.58 ± 0.02	1.71 ± 0.04	1.45 ± 0.05	1.44 ± 0.01	1.54 ± 0.03
	75	0.7880	1.028	1.84 ± 0.02	1.65 ± 0.03	–	1.47 ± 0.01	–	–	1.35 ± 0.01	–	–
	150	0.7940	1.090	1.77 ± 0.01	1.57 ± 0.01	1.71 ± 0.04	1.39 ± 0.01	–	1.54 ± 0.01	1.29 ± 0.01	1.28 ± 0.01	1.39 ± 0.01
318.15	1	0.7686	0.7450	2.38 ± 0.04	2.16 ± 0.03	2.35 ± 0.06	1.94 ± 0.03	–	2.14 ± 0.05	1.78 ± 0.03	–	1.87 ± 0.03
	75	0.7756	0.7989	2.23 ± 0.02	2.05 ± 0.01	–	1.83 ± 0.01	–	–	1.68 ± 0.01	–	–
	150	0.7821	0.8513	2.12 ± 0.02	1.94 ± 0.01	2.06 ± 0.02	1.73 ± 0.01	–	1.90 ± 0.02	1.58 ± 0.01	–	1.70 ± 0.02
333.15	1	0.7557	0.5872	2.89 ± 0.06	2.63 ± 0.06	2.68 ± 0.06	2.41 ± 0.04	2.43 ± 0.06	2.50 ± 0.05	2.18 ± 0.03	2.17 ± 0.05	2.27 ± 0.03
	75	0.7631	0.6332	2.72 ± 0.04	2.51 ± 0.04	–	2.22 ± 0.02	–	–	2.03 ± 0.02	–	–
	150	0.7700	0.6780	2.57 ± 0.05	2.37 ± 0.02	2.42 ± 0.02	2.10 ± 0.01	–	2.24 ± 0.03	1.93 ± 0.01	1.97 ± 0.01	2.02 ± 0.02

[†] Density estimated by Tait [53] and the Eykman [54,55] methods.
[*] Viscosity estimated by the Mamedov equation[56]
[††] Standard uncertainty.

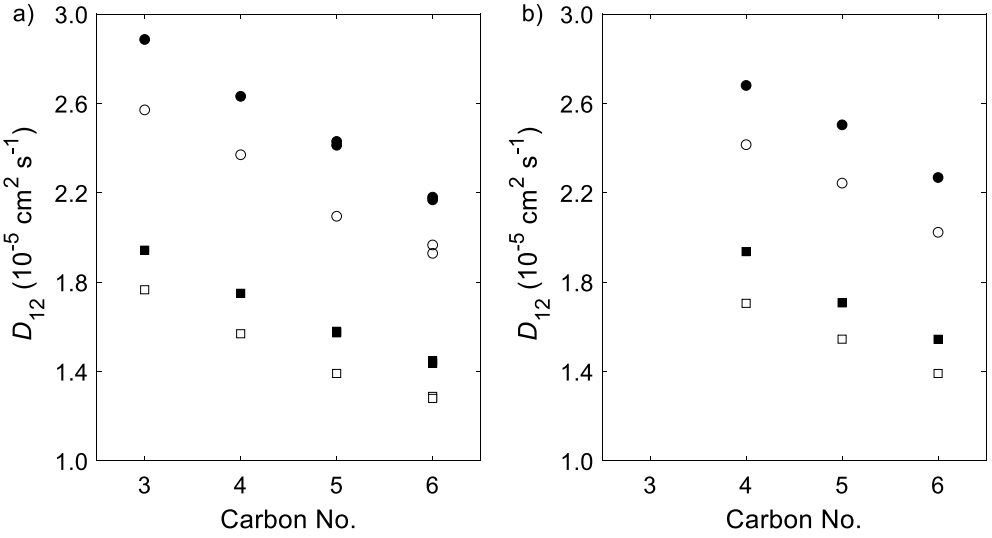

Fig. 1. Diffusion coefficients (D_{12}) *versus* number of carbons of the studied (a) ketones and (b) aldehydes at: (■) 303.15 K and 1 bar; (□) 303.15 K and 150 bar; (●) 333.15 K and 1 bar; and (○) 333.15 K and 150 bar.

4.3.3. D_{12} trends of isomers

It was found that the D_{12} values of the aldehydes/ketones isomers are statistically different with 95 % confidence, except for butanal/butanone at 333.15 K and 1 bar (see Table A.1 in Appendix A). As for the C5 and C6 isomeric ketones, the D_{12} values were found to be statistically the same, hence only a few measurements were performed. The exception was for hexan-2-one/hexan-3-one isomers at 333.15 K and 1 bar, probably due to experimental error. The similarities between D_{12} values of the ketone isomers can also be found in SC-CO_2 as reported by Funazukuri *et al.* [26].

Getting into a more detailed analysis, the position of the functional group of ketones seems to not affect D_{12}. In both pentanone (C5) and hexanone (C6) isomers, the D_{12} values do not differ at the studied conditions (aside the above mentioned hexan-2-one/hexan-3-one isomers at 333.15 K and 1 bar). This is in accordance with the similar Lennard-Jones diameters of the isomer pairs (see Table 2). As for the isomeric aldehydes/ketones, the D_{12} values differ being consistently higher for the former. The difference between the functional isomers is in average 6.7 % higher, with a maximum difference of 11.0 % observed between pentanal and pentan-2-one at 303.15 K and 150 bar. Although small, this difference should not be disregarded and can be explained by the smaller size of aldehydes in comparison to the corresponding isomeric ketones (see the estimated Lennard-Jones diameters (σ_{LJ}) found in Table 2).

4.3.4. D_{12} hydrodynamic trends

In Fig. 2 the measured D_{12} values were plotted against Stokes-Einstein abscissas, T/μ_1. The coefficient of determination, R^2, for the linear relationship is generally high for all studied substances. The R^2 values were found to be between 0.9703 and 1, with the lowest value corresponding to butanal and the highest to pentan-3-one. However, in the latter case this does not indicate a perfect fitting since only two conditions have been measured. As for the y-intersect, small deviations from zero are present for all systems, with values between 4.584×10^{-6} and 8.794×10^{-6} cm^2 s^{-1}, which are in accordance with nonconformities found in other studied systems [52,61]. All the results are compiled in Table A.2 (See Appendix A).

4.3.5. D_{12} trend with free volume

As for the free volume influence, Fig. 3 shows that the expected trend between $D_{12}T^{-0.5}$ and V_1 was verified for all systems. As stated by the free volume DHB correlation [37–39] (Equation (9)), the values of D_{12} should increase with V_1. The general temperature and pressure effect upon D_{12} can be anticipated by their influence upon the solvent molar volume, *i.e.*: as temperature increases, V_1 also increases enhancing the effect of T on D_{12}; and as pressure increases, free volume decreases causing D_{12} to decrease.

Table 2
Physical properties of the compounds studied in this work, namely: molecular weight (M), critical pressure (P_c), critical temperatures (T_c), critical volume (V_c), Lennard-Jones diameter (σ_{LJ}), Lennard-Jones energy parameter (ε_{LJ}/k_B), and molar volume at normal boiling temperature (V_{bp}).

	M (g mol^{-1})	P_c (bar)	T_c (K)	V_c (cm^3 mol^{-1})	σ_{LJ} (Å)	ε_{LJ}/k_B (K)	V_{bp} [f] (cm^3 mol^{-1})
Propanone	58.08	47.0[a]	508.10[a]	209[a]	4.67012[b]	332.97[b]	77.0
Butanal	72.11	43.2[c]	537.20[c]	258[c]	5.18098[d]	415.79[d]	96.0
Butanone	72.11	42.1[a]	536.80[a]	267[a]	5.22195[d]	415.48[d]	99.5
Pentanal	86.13	39.7[c]	566.10[c]	313[c]	5.40807[d]	438.16[d]	117.5
Pentan-2-one	86.13	36.9[a]	561.10[a]	301[a]	5.51733[d]	434.29[d]	112.8
Pentan-3-one	86.13	37.3[a]	561.50[a]	336[a]	5.49858[d]	434.21[d]	126.6
Hexanal	100.16	34.6[c]	591.00[c]	369[c]	5.71919[d]	457.43[d]	139.7
Hexan-2-one	100.16	33.2[a]	587.00[e]	378[e]	5.78012[d]	454.34[d]	143.2
Hexan-3-one	100.16	33.2[a]	582.00[e]	378[e]	5.76497[d]	450.47[d]	143.2
Ethanol	46.07	61.4[a]	513.90[a]	167.1[a]	4.23738[b]	1291.41[b]	–

[a] Taken from Reid *et al.* [62].
[b] Taken from Liu *et al.* 1998 [58].
[c] Taken from Yaws 2008 [63].
[d] Calculated by equations (8) and (9) from Zêzere *et al.* [36].
[e] Taken from Poling *et al.* [33].
[f] Calculated by the Tyn-Calus equation [50].

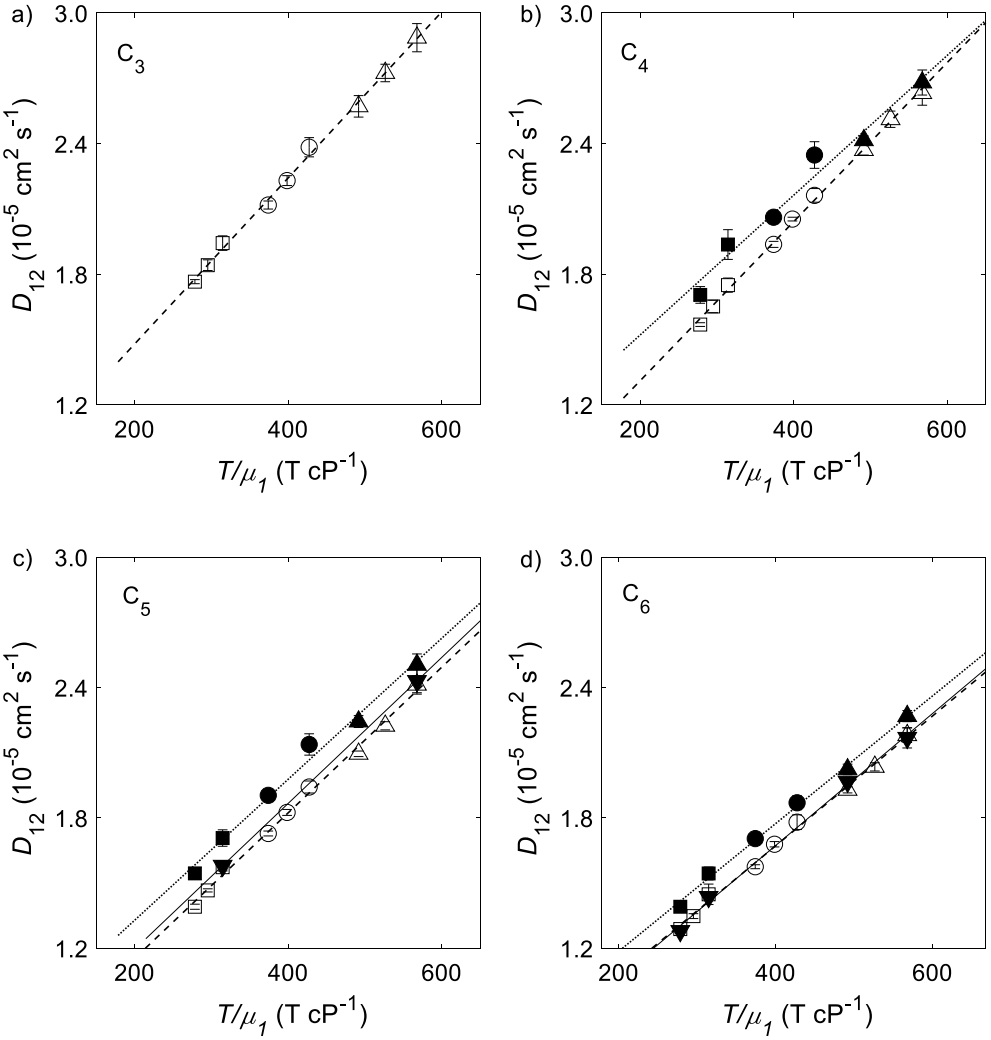

Fig. 2. Stokes-Einstein representation of D_{12} of a) propanone; b) butanone (white symbols) and butanal (full symbols); c) pentan-2-one (white symbols), pentanal (black symbols) and pentan-3-one (▼); and d) hexan-2-one (white symbols), hexanal (black symbols) and hexan-3-one (▼) in ethanol at $T = 303.15$ K (□ and ■), 318.15 K (△ and ▲) and 333.15 K (○ and ●), from 1 bar to 150 bar. Trend lines for every compound are represented. Error bars were calculated with 4 to 6 replicas.

4.4. Modelling results and discussion

The predictive and correlative capabilities of five models from the literature (WC, TLSM, TLSM$_d$, DHB, RG, and the ML-GB algorithm) were evaluated using the experimental data presented in this work. The required properties of the models can be found in Table 3 along with their references and/or the methods used for their estimation. The modelling results are listed in Table 3 and

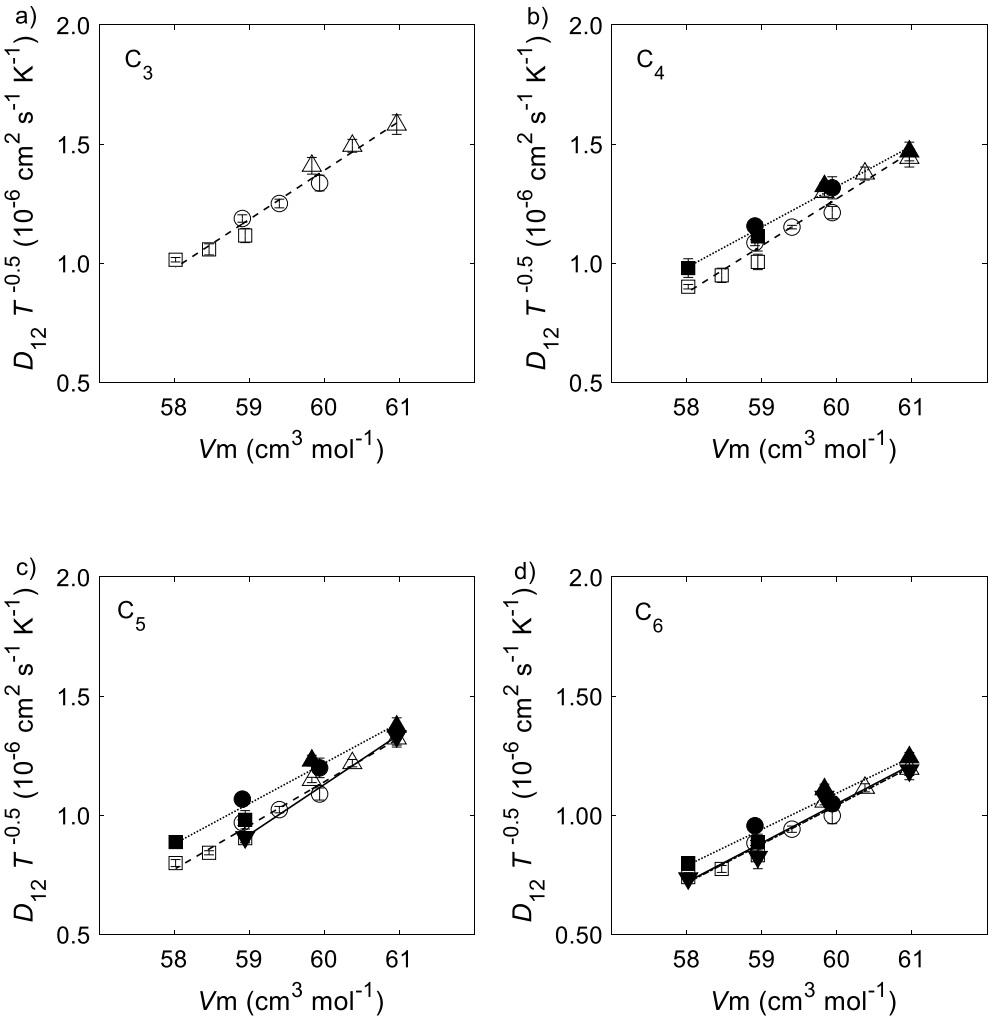

Fig. 3. Free-volume representation of D_{12} of a) propanone; b) butanone (white symbols) and butanal (full symbols); c) pentan-2-one (white symbols), pentanal (black symbols) and pentan-3-one (▼); and d) hexan-2-one (white symbols), hexanal (black symbols) and hexan-3-one (▼) in ethanol at $T = 303.15$ K (□ and ■), 318.15 K (△ and ▲) and 333.15 K (○ and ●), from 1 bar to 150 bar. Trend lines for every compound are represented. Error bars were calculated with 4 to 6 replicas.

graphical representations can be found in Figs. 4 and 5. In Fig. A.2 it is presented a global comparison between the calculated diffusivities of butanone and butanal achieved by the various models, using Stokes-Einstein coordinates, except ML-GB as it is already provided in Fig. 5. Overall, most of the models showed at least satisfactory results except the WC equation and ML-GB algorithm where some peculiarities were identified.

For the predictive TLSM model, the performance is good for both chemical families (AARD values between 5.12 % and 11.24 %) being slightly better for the investigated ketones: the AARD values are below 10 % in the case of ketones and slightly above 10 % for aldehydes. The modelling performance was further improved with the introduction of the binary parameter $k_{12,d}$, which corresponds to the $TLSM_d$ model. The good TLSM results

Table 3
Calculated deviations (AARD, %) and model parameters of the various D_{12} modeling approaches.

	WC [32,33]	TLSM [34–36]	$TLSM_d$ [34–36]		DHB [37–39]			RG [40]			ML-GB [41]
	AARD (%)	AARD (%)	AARD (%)	$k_{12,d}$ (adm)	AARD (%)	B_{DHB} (mol cm^{-1} s^{-1}K$^{-0.5}$)	V_D (cm^{3}mol^{-1})	AARD (%)	k_{12} (adm)	B_{12} (adm)	AARD (%)
Propanone	19.55	7.63	1.03	−0.037586	2.44	2.060×10^{-7}	53.26	1.34	−0.58648	−0.66123	5.91
Butanone	24.21	6.07	1.56	0.030375	2.80	1.977×10^{-7}	53.57	1.73	−0.63084	−0.77751	17.08
Pentan-2-one	21.32	5.12	1.69	0.024972	2.37	1.838×10^{-7}	53.80	1.52	−0.77701	−1.00041	21.91
Pentan-3-one	27.16	6.60	3.04	0.018526	0.00	2.100×10^{-7}	54.62	0.00	−0.96578	−1.40293	30.41
Hexan-2-one	25.63	5.19	1.41	0.026604	2.33	1.631×10^{-7}	53.61	1.43	−0.71291	−0.82359	12.84
Hexan-3-one	25.87	4.98	2.51	0.013565	3.65	1.646×10^{-7}	53.63	2.14	−0.72274	−0.83883	11.27
Butanal	26.83	10.88	1.36	0.056583	1.47	1.702×10^{-7}	52.23	0.74	−0.33193	0.27796	14.36
Pentanal	29.21	11.24	0.83	0.056748	2.40	1.696×10^{-7}	52.82	1.29	−0.53763	−0.55834	32.11
Hexanal	28.84	10.10	0.64	0.051472	2.74	1.522×10^{-7}	52.82	1.40	−0.55834	−0.49549	4.67

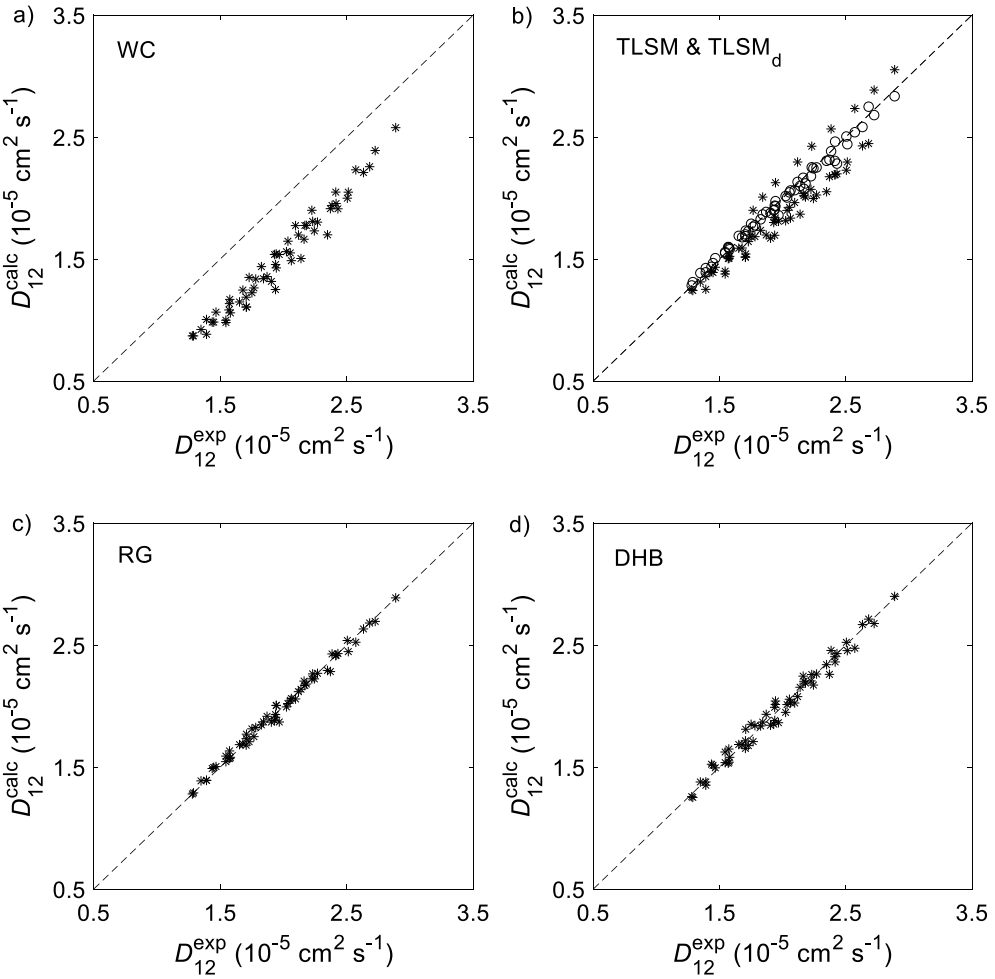

Fig. 4. Calculated (calc) *versus* experimental (exp) D_{12}. Calculated diffusion by: a) Wilke-Chang equation, b) TLSM (*) and TLSM$_d$ (○) models, c) Rice and Gray model, and d) DHB equation.

are surprising since this model was devised for Lennard-Jones fluids [34,58], thus it is expected to fail when estimating and correlating D_{12} data of hydrogen-bonding molecules like the solutes and solvent (ethanol) used in this study. As for the well-known Wilke-Chang equation, the AARD values are between 19.55 % and 29.21 %, which are far superior to those of TLSM model. Furthermore, as evidenced in Fig. 4a the calculated D_{12} values are always underestimated. Hence for pure prediction of D_{12} the TLSM model should be selected. One should also take note that the AARD values for the TLSM model are independent of the number of carbons of the solutes. Therefore, it should be expected to perform as well for larger ketones and aldehydes.

Concerning the 2-parameter correlations of DHB [37–39] and Rice and Grey [40], the AARD of pentan-3-one was naturally zero since only two data points were available. For the other solutes, these models accomplish good results with AARD values between 0.74 % and 3.65 %. Nevertheless, it should be emphasized that the Rice and Grey correlation achieves slightly lower deviations for all the solutes studied, naturally at a cost of increasing complexity. Comparing these results with the ones achieved by the one-parameter TLSM$_d$ correlation, one may observe that their AARD values are very similar even though the former has only one adjustable parameter. In any case the three correlations may be recommended for D_{12} estimation of aldehydes and ketones in liquid ethanol. The D_{12}^{calc} *versus* D_{12}^{exp} subplots shown in Fig. 4 illustrates the models performance.

Before concluding the discussion of classical models, it is interesting to analyze the V_D parameter of DHB correlation, which is theoretically attributed to the solvent (*i.e.*, ethanol) as $V_1 - V_D$ represents its free volume available for diffusion. Following Dymond [38], V_D can be calculated as function of the close-packed molar volume of the solvent (V_0) by $V_D = 1.384V_0$, where V_0 may be temperature dependent [64]. For the operating conditions of this work, the estimated values of V_D range between 45.83 and 46.71 cm^3 mol^{-1}, *i.e.* they are 12.47 to 14.11 % lower than those fitted to the experimental data and listed in Table 3. Furthermore, if such estimated V_D values are fixed in Equation (9) and only B_{DHB} is adjusted, the final AARDs for the resulting 1-parameter DHB correlation are 5.94 % for ketones and 4.11 % for aldehydes, which are *ca.* the double of the 2.48 % and 2.20 % found for the 2-parameter model.

As for the machine learning algorithm ML-GB Polar, low AARD values are achieved only for two of the solutes, namely, propanone and hexanal. The remaining values are above 10 %, with both hexanone molecules having similar values as they are isomeric ketones. Moreover, pentanal and the two pentanone isomers achieved the highest AARD with a maximum deviation value of 49.28 % for pentanal at 303.15 K and 1 bar. As for the model capability of translating D_{12} as function of T and P, it seems to show the correct trend for the former variable (*i.e.*, D_{12} increases with T) but not for the latter. In fact, D_{12} in some conditions increases with P contrary to what is

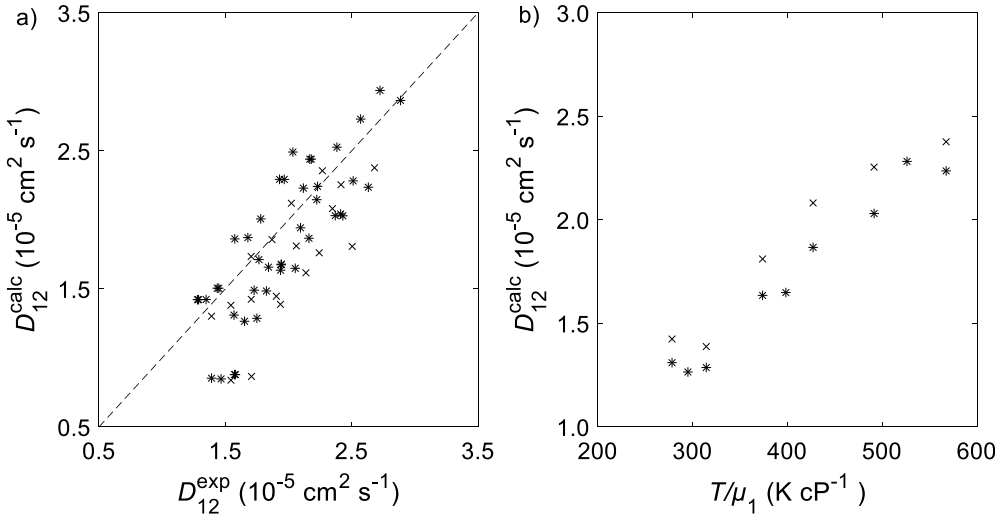

Fig. 5. Graphical representation of ML-GB calculations for D_{12} of butanone (*) and butanal (×): a) calculated (calc) *versus* experimental (exp) D_{12}, and b) Stokes-Einstein representation.

expected. These ML-GB trends can be evidenced in Fig. 5 where D_{12}^{calc} *versus* D_{12}^{exp}, and the Stokes-Einstein representation of both butanone and butanal diffusivities are plotted.

5. Conclusions

The binary diffusion coefficients, D_{12}, of short chains (C3-C6) ketones and aldehydes in compressed liquid ethanol were measured by the chromatographic peak broadening technique at temperatures between 303.15 K and 333.15 K and pressures up to 150 bar. The determined values ranged between 1.28×10^{-5} cm^2 s^{-1} and 2.89×10^{-5} cm^2 s^{-1} for the studied ketones and from 1.39×10^{-5} cm^2 s^{-1} to 2.68×10^{-5} cm^2 s^{-1} for the aldehydes.

The behavior of D_{12} as function of temperature, pressure, free volume, and Stokes-Einstein variables, for all investigated ketones and aldehydes, was analyzed and followed reliable and expected trends. Furthermore, the isomeric saturated ketones showed the same diffusion coefficients, while aldehydes/ketones isomers exhibit different diffusivities.

Concerning modelling results, the DHB, $TLSM_d$, and Rice and Gray correlations achieved accurate results with average deviations as low as 0.64 % and maximum value of 3.65 %. As for the purely predictive TLSM model, it achieved good results with errors between 4.98 % and 11.24 %, considerably better than the well-known Wilke-Chang model (errors between 19.55 % and 29.21 %). As for a machine learning algorithm (ML-Polar), it showed good predictive capability for some of solutes, but fails to correctly translate the pressure influence for some data points. In the whole, the TLSM model should be the preferred approach for D_{12} prediction of linear unsaturated aldehydes and ketones.

CRediT authorship contribution statement

Bruno Zêzere: Methodology, Investigation, Writing – original draft. **Simon Buchgeister:** Investigation, Writing – original draft. **Sofia Faria:** Investigation. **Inês Portugal:** Resources, Writing – review & editing, Formal analysis. **José R. B. Gomes:** Supervision, Resources, Writing – review & editing. **Carlos Manuel Silva:** Supervision, Conceptualization, Resources, Writing – review & editing, Funding acquisition, Formal analysis.

Declaration of Competing Interest

The authors declare that they have no known competing financial interests or personal relationships that could have appeared to influence the work reported in this paper.

Acknowledgments

This work was developed within the scope of the project CICECO-Aveiro Institute of Materials, UIDB/50011/2020, UIDP/50011/2020 & LA/P/0006/2020, financed by national funds through the FCT/MEC (PIDDAC). Bruno Zêzere thanks FCT for the PhD grant SFRH/BD/137751/2018.

Appendix

Table A1
p-values from the analysis of variance (ANOVA; 95 % confidence interval) between the D_{12} values of the different isomers in compressed liquid ethanol.

T(K)	P(bar)	Butanal *vs* Butanone	Pentanal *vs* Pentan-2-one	Hexanal *vs* Hexan-2-one	Pentan-3-one *vs* Pentan-2-one	Hexan-2-one *vs* Hexan-3-one	Pentanal *vs* Pentan-3-one	Hexanal *vs* Hexan-2-one
303.15	1	0.000	0.000	0.003	0.589	0.720	0.000	0.000
303.15	150	0.000	0.000	0.000	–	0.217	–	0.000
318.15	1	0.000	0.000	0.003	–	–	–	–
318.15	150	0.000	0.000	0.000	–	–	–	–
333.15	1	0.203	0.001	0.000	0.522	0.720	0.023	0.004
333.15	150	0.006	0.000	0.000	–	0.006	–	0.001

Table A2
Parameters of the hydrodynamic Equation (A.1) of the studied solutes in compressed liquid ethanol: slope ($m \pm \Delta m$), y-intercept ($b \pm \Delta b$), coefficient of determination (R^2), and p-value (95 % confidence interval) of m and b.

	$m \pm \Delta\, m$ (10^{-8} cP cm^2 K^{-1} s^{-1})	$b \pm \Delta\, b$ (10^{-6}cm^2 s^{-1})	R^2	m p-value	b p-value
Propanone	3.813 ± 0.075	7.185 ± 0.311	0.9973	2.879×10^{-10}	7.558×10^{-8}
Butanone	3.654 ± 0.070	5.805 ± 0.281	0.9988	1.821×10^{-10}	1.562×10^{-7}
Pentan-2-one	3.351 ± 0.094	4.840 ± 0.395	0.9945	3.591×10^{-9}	5.522×10^{-6}
Pentan-3-one	3.358 ± 0.000	5.244 ± 0.000	1.0000	–	–
Hexan-2-one	2.988 ± 0.074	4.770 ± 0.309	0.9958	1.447×10^{-9}	1.160×10^{-6}
Hexan-3-one	3.038 ± 0.115	4.584 ± 0.493	0.9972	1.422×10^{-3}	1.138×10^{-2}
Butanal	3.210 ± 0.281	8.794 ± 1.181	0.9703	3.335×10^{-4}	1.735×10^{-3}
Pentanal	3.224 ± 0.184	6.812 ± 0.775	0.9872	6.123×10^{-5}	9.256×10^{-4}
Hexanal	2.938 ± 0.087	5.995 ± 0.367	0.9965	4.629×10^{-6}	8.206×10^{-5}

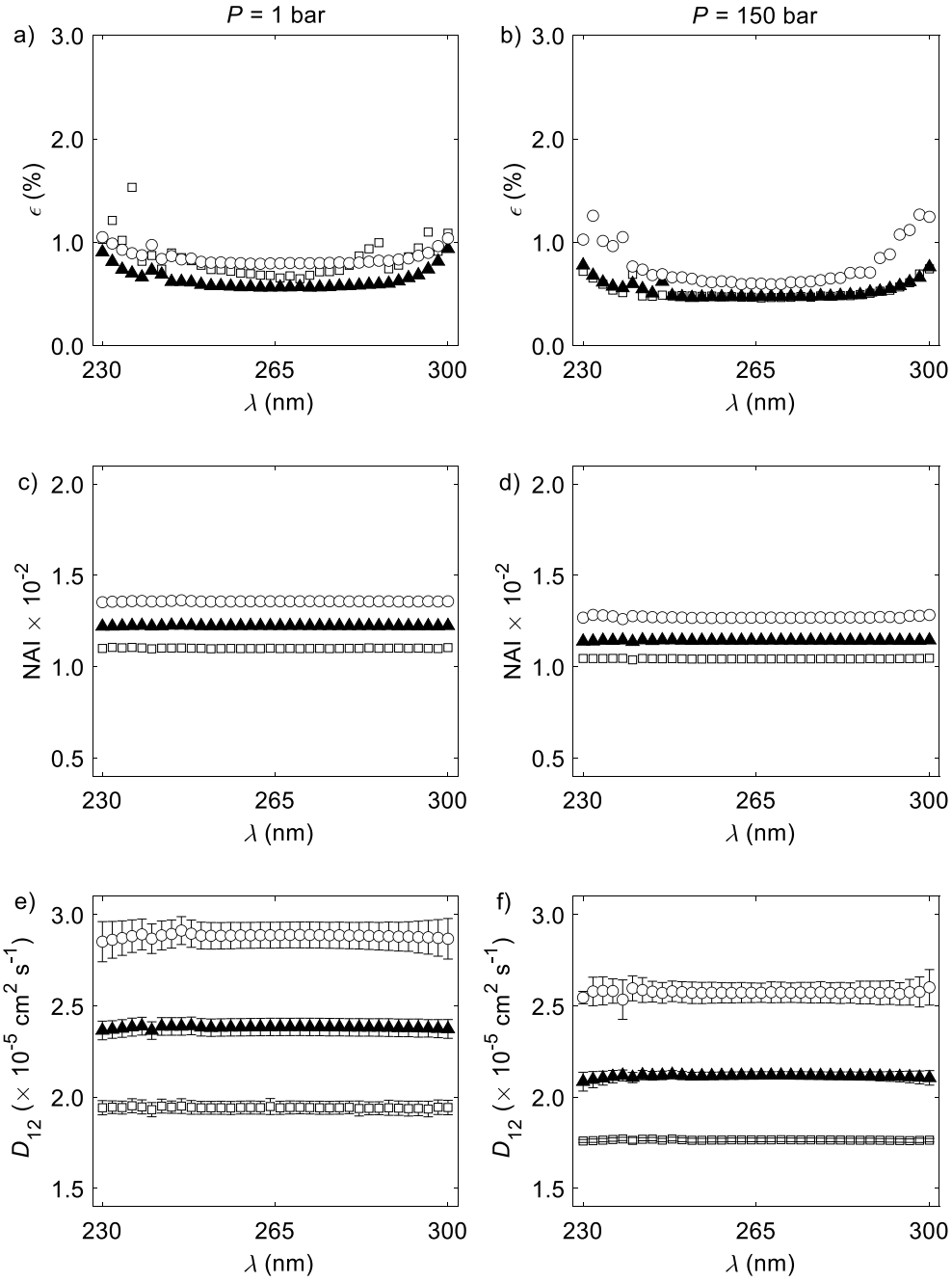

Fig. A1. Wavelength study of propanone in ethanol at 303.15 K (□), 318.15 K (▲) and 333.15 K (○) for 1 bar (a, c and e) and 150 bar (b, d and f). In (a) and (b), the root mean square error (ε) *versus* wavelength (λ) is shown; in (c) and (d), NAI = Abs_{max}/A_{peak} *versus* λ is plotted; and in (e) and (f), diffusion coefficient *versus* λ is shown.

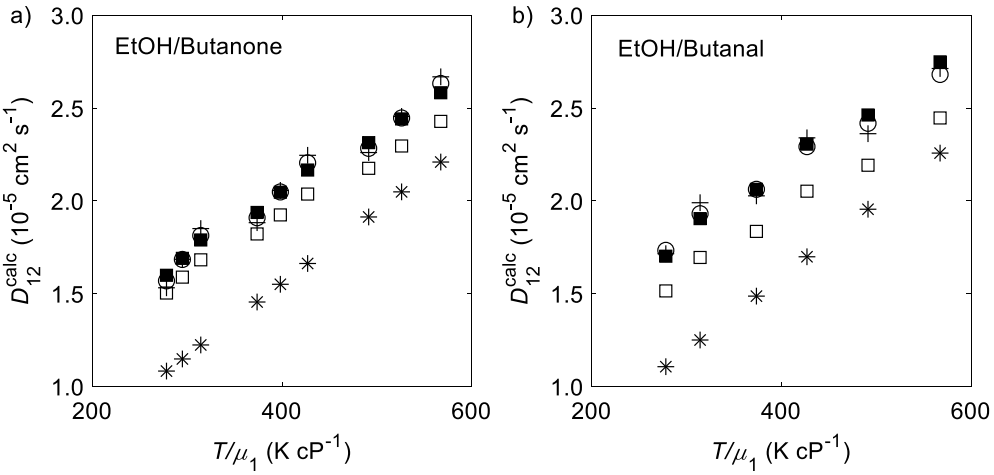

Fig. A2. Stokes-Einstein plot of the calculated diffusivities of (a) butanone and (b) butanal in liquid ethanol. Models: (*) Wilke-Chang, (□) TLSM, (■) $TLSM_d$, (+) DHB and (○) Rice and Gray.

$$D_{12} = \frac{T}{\mu_1} m + b \tag{A1}$$

References

[1] E.L. Cussler, Diffusion: Mass Transfer in Fluid Systems, Third ed., Cambridge University Press, Cambridge, 2009.
[2] A. Vignes, Diffusion in binary solutions. Variation of diffusion coefficient with composition, Ind. Eng. Chem. Fundam. 5 (1966) 189–199, https://doi.org/10.1021/i160018a007.
[3] R. Taylor, R. Krishna, Multicomponent Mass Transfer, John Wiley & Sons Inc, New York, 1993.
[4] R. Krishna, J.A. Wesselingh, The Maxwell-Stefan approach to mass transfer, Chem. Eng. Sci. 52 (1997) 861–911, https://doi.org/10.1016/S0009-2509(96)00458-7.
[5] G. Taylor, Dispersion of soluble matter in solvent flowing slowly through a tube, Proc. R. Soc. A Math. Phys. Eng. Sci. 219 (1953) 186–203, https://doi.org/10.1098/rspa.1953.0139.
[6] G. Taylor, Diffusion and mass transport in tubes, Proc. Phys. Soc. Sect. B 67 (1954) 857–869, https://doi.org/10.1088/0370-1301/67/12/301.
[7] G. Taylor, The dispersion of matter in turbulent flow through a pipe, Proc. R. Soc. A Math. Phys. Eng. Sci. 223 (1954) 446–468, https://doi.org/10.1098/rspa.1954.0130.
[8] R. Aris, On the dispersion of a solute by diffusion, convection and exchange between phases, Proc. R. Soc. A Math. Phys. Eng. Sci. 252 (1959) 538–550, https://doi.org/10.1098/rspa.1959.0171.
[9] C. Kohlpaintner, M. Schulte, J. Falbe, P. Lappe, J. Weber, G.D. Frey, Aliphatic Aldehydes, Ullmann's Encyclopedia of Industrial Chemistry, Wiley-VCH Verlag GmbH & Co. KGaA, Weinheim, Germany, 2013, https://doi.org/10.1002/14356007.a01_321.pub3.
[10] V.J. Feron, H.P. Til, F. de Vrijer, R.A. Woutersen, F.R. Cassee, P.J. van Bladeren, Aldehydes: occurrence, carcinogenic potential, mechanism of action and risk assessment, Mutat. Res. Toxicol. 259 (1991) 363–385, https://doi.org/10.1016/0165-1218(91)90128-9.
[11] M. Shui, T. Feng, Y. Tong, H. Zhuang, C. Lo, H. Sun, L. Chen, S. Song, Characterization of key aroma compounds and construction of flavor base module of Chinese sweet oranges, Molecules 24 (2019) 2384, https://doi.org/10.3390/molecules24132384.
[12] T.W.G. Solomons, C.B. Fryhle, Organic Chemistry, Tenth ed., John Wiley & Sons, inc., Hoboken, 2011.
[13] L. Zhao, M. Zhang, H. Wang, Inhibition of the fishy odor from boiled crab meatballs during storage via novel combination of radio frequency and carbon dots, Food Control. 136 (2022), https://doi.org/10.1016/j.foodcont.2022.108843 108843.
[14] A.S. Khan, S. Ali, in: Preharvest Modulation of Postharvest Fruit and Vegetable Quality, Elsevier, 2018, pp. 209–255.
[15] J. Song, R. Leepipattanawit, W. Deng, R.M. Beaudry, Hexanal vapor is a natural, metabolizable fungicide: inhibition of fungal activity and enhancement of aroma biosynthesis in apple slices, Am. Soc. Hortic. Sci. 121 (1996) 937–942, https://doi.org/10.21273/JASHS.121.5.937.
[16] L.-T. Lim, Gases and Vapors Used in Food, in: P. Varelis, L. Melton, F. Shahidi (Eds.), Encyclopedia of Food Chemistry, Elsevier, 2019, pp. 114–120.
[17] S.J. Klein, Butyraldehyde, in: P. Wexler (Ed.), Encyclopedia of Toxicology, Third ed., Elsevier, 2014, pp. 595–596, https://doi.org/10.1016/B978-0-12-386454-3.00264-5.
[18] A. Schmidt, Ketone, RÖMPP. (2006). https://roempp.thieme.de/lexicon/RD-11-00957 (accessed April 24, 2022).
[19] H. Siegel, M. Eggersdorfer, Ketones, in: Ullmann's Encyclopedia of Industrial Chemistry, Wiley-VCH Verlag GmbH & Co., KGaA, Weinheim, Germany, 2000, https://doi.org/10.1002/14356007.a15_077.
[20] A. Behr, D.W. Agar, J. Jörissen, A.J. Vorholt, Einführung in die Technische Chemie, Springer Berlin Heidelberg, Berlin, Heidelberg, 2016.
[21] A. Kopner, A. Hamm, J. Ellert, R. Feist, G.M. Schneider, Determination of binary diffusion coefficients in supercritical chlorotrifluoromethane and sulfurhexafluoride with supercritical fluid chromatography (SFC), Chem. Eng. Sci. 42 (1987) 2213–2218, https://doi.org/10.1016/0009-2509(87)85043-1.
[22] M.T. Tyn, W.F. Calus, Temperature and concentration dependence of mutual diffusion coefficients of some binary liquid systems, J. Chem. Eng. Data 20 (1975) 310–316, https://doi.org/10.1021/je60066a009.
[23] T. Funazukuri, N. Nishimoto, N. Wakao, Binary diffusion coefficients of organic compounds in hexane, dodecane, and cyclohexane at 303.2-333.2 K and 16.0 MPa, J. Chem. Eng. Data 39 (4) (1994) 911–915, https://doi.org/10.1021/je00016a062.
[24] T. Funazukuri, C.Y. Kong, S. Kagei, Binary diffusion coefficients of acetone in carbon dioxide at 308.2 and 313.2 K in the pressure range from 7.9 to 40 MPa, Int. J. Thermophys. 21 (2000) 651–669, https://doi.org/10.1023/A:1006637401868.
[25] P.R. Sassiat, P. Mourier, M.H. Caude, R.H. Rosset, Measurement of diffusion coefficients in supercritical carbon dioxide and correlation with the equation of Wilke and Chang, Anal. Chem. 59 (1987) 1164–1170, https://doi.org/10.1021/ac00135a020.
[26] T. Funazukuri, C.Y. Kong, S. Kagei, Infinite-dilution binary diffusion coefficients of 2-propanone, 2-butanone, 2-pentanone, and 3-pentanone in CO_2, Int. J. Thermophys. 21 (2000) 1279–1290, https://doi.org/10.1023/A:1006749309979.
[27] C.Y. Kong, T. Funazukuri, S. Kagei, Chromatographic impulse response technique with curve fitting to measure binary diffusion coefficients and retention factors using polymer-coated capillary columns, J. Chromatogr. A 1035 (2004) 177–193, https://doi.org/10.1016/j.chroma.2004.02.067.
[28] H. Nishiumi, M. Fujita, K. Agou, Diffusion of acetone in supercritical carbon dioxide, Fluid Phase Equilib. 117 (1996) 356–363, https://doi.org/10.1016/0378-3812(95)02972-9.
[29] J.J. Suárez, I. Medina, J.L. Bueno, Diffusion coefficients in supercritical fluids: available data and graphical correlations, Fluid Phase Equilib. 153 (1998) 167–212, https://doi.org/10.1016/S0378-3812(98)00403-8.
[30] T. Funazukuri, Measurements of binary diffusion coefficients of 20 organic compounds in CO_2 at 313.2 K and 16.0 MPa, J. Chem. Eng. Japan 29 (1996) 191–192, https://doi.org/10.1252/jcej.29.191.
[31] N. Dahmen, A. Dulberg, G.M.M. Schneider, Determination of binary diffusion coefficients in supercritical carbon dioxide with supercritical fluid chromatography (SFC), Ber. Bunsenges. Phys. Chem. 94 (1990) 384–386, https://doi.org/10.1016/S0021-9673(01)93076-6.
[32] C.R. Wilke, P. Chang, Correlation of diffusion coefficients in dilute solutions, AIChE J. 1 (1955) 264–270, https://doi.org/10.1002/aic.690010222.
[33] B.E. Poling, J.M. Prausnitz, J.P. O'Connell, The Properties of Gases and Liquids, Fifth ed., The McGraw-Hill Companies Inc, New York, 2001.
[34] H. Liu, C.M. Silva, E.A. Macedo, New equations for tracer diffusion coefficients of solutes in supercritical and liquid solvents based on the Lennard-Jones fluid model, Ind. Eng. Chem. Res. 36 (1997) 246–252, https://doi.org/10.1021/ie9602318.
[35] A.L. Magalhães, S.P. Cardoso, B.R. Figueiredo, F.A. Da Silva, C.M. Silva, Revisiting the Liu-Silva-Macedo model for tracer diffusion coefficients of supercritical,

liquid, and gaseous systems, Ind. Eng. Chem. Res. 49 (2010) 7697–7700, https://doi.org/10.1021/ie1009475.
[36] B. Zêzere, I. Portugal, J.R.B. Gomes, C.M. Silva, Revisiting Tracer Liu-Silva-Macedo model for binary diffusion coefficient using the largest database of liquid and supercritical systems, J. Supercrit. Fluids 168 (2021), https://doi.org/10.1016/j.supflu.2020.105073 105073.
[37] C.M. Silva, H. Liu, Modelling of transport properties of hard sphere fluids and related systems and its applications, in: Á. Mulero (Ed.), Lecture Notes in PhysicsTheory and Simulation of Hard-Sphere Fluids and Related Systems, Springer Berlin Heidelberg, Berlin, Heidelberg, 2008, pp. 383–492.
[38] J.H. Dymond, Corrected Enskog theory and transport coefficients of liquids, J. Chem. Phys. 60 (1974) 969–973, https://doi.org/10.1063/1.1681175.
[39] J.H. Dymond, E. Bich, E. Vogel, W.A. Wakeham, V. Vesovic, M.J. Assael, Dense fluids, in: J. Millat, J.H. Dymond, C.A.N.d. Castro, W.A. Wakeham (Eds.), Transport Properties of Fluids: Their Correlation, Prediction and Estimation, Cambridge University Press, 1996, pp. 66–112.
[40] B. Zêzere, I. Portugal, J.R.B. Gomes, C.M. Silva, A simplified correlation for tracer diffusion coefficients in polar and non-polar dense solvents, Materials 15 (2022) 6416, https://doi.org/10.3390/ma15186416.
[41] J.P.S. Aniceto, B. Zêzere, C.M. Silva, Predictive models for the binary diffusion coefficient at infinite dilution in polar and nonpolar fluids, Materials 14 (2021) 542, https://doi.org/10.3390/ma14030542.
[42] B. Zêzere, J. Iglésias, I. Portugal, J.R.B. Gomes, C.M. Silva, Diffusion of quercetin in compressed liquid ethyl acetate and ethanol, J. Mol. Liq. (2020), https://doi.org/10.1016/j.molliq.2020.114714 114714.
[43] G. Cai, W. Katsumata, I. Okajima, T. Sako, T. Funazukuri, C.Y. Kong, Determination of diffusivities of triolein in pressurized liquids and in supercritical CO_2, J. Mol. Liq. 354 (2022), https://doi.org/10.1016/j.molliq.2022.118860 118860.
[44] A. Alizadeh, C.A. Nieto de Castro, W.A. Wakeham, The theory of the Taylor dispersion technique for liquid diffusivity measurements, Int. J. Thermophys. 1 (1980) 243–284, https://doi.org/10.1007/BF00517126.
[45] T. Funazukuri, C.Y. Kong, S. Kagei, Impulse response techniques to measure binary diffusion coefficients under supercritical conditions, J. Chromatogr. A 1037 (2004) 411–429, https://doi.org/10.1016/j.chroma.2004.03.043.
[46] K.K. Liong, P.A. Wells, N.R. Foster, Diffusion in supercritical fluids, J. Supercrit. Fluids 4 (1991) 91–108, https://doi.org/10.1016/0896-8446(91)90037-7.
[47] O. Levenspiel, W.K. Smith, Notes on the diffusion-type model for the longitudinal mixing of fluids in flow, Chem. Eng. Sci. 50 (1995) 3891–3896, https://doi.org/10.1016/0009-2509(96)81817-3.
[48] J.A. Moulijn, R. Spijker, J.F.M. Kolk, Axial dispersion of gases flowing through coiled columns, J. Chromatogr. A 142 (1977) 155–166, https://doi.org/10.1016/S0021-9673(01)92035-7.
[49] T. Funazukuri, C.Y. Kong, S. Kagei, Binary diffusion coefficients in supercritical fluids: recent progress in measurements and correlations for binary diffusion coefficients, J. Supercrit. Fluids 38 (2006) 201–210, https://doi.org/10.1016/j.supflu.2006.02.016.
[50] M.T. Tyn, W.F. Calus, Estimating liquid molal volume, Processing 21 (1975) 16–17.
[51] A.L. Magalhães, P.F. Lito, F.A. Da Silva, C.M. Silva, Simple and accurate correlations for diffusion coefficients of solutes in liquids and supercritical fluids over wide ranges of temperature and density, J. Supercrit. Fluids 76 (2013) 94–114, https://doi.org/10.1016/j.supflu.2013.02.002.
[52] B. Zêzere, J.M. Silva, I. Portugal, J.R.B. Gomes, C.M. Silva, Measurement of astaxanthin and squalene diffusivities in compressed liquid ethyl acetate by Taylor-Aris dispersion method, Sep. Purif. Technol. 234 (2020), https://doi.org/10.1016/j.seppur.2019.116046 116046.
[53] M.J. Assael, J.H. Dymond, S.K. Polimatidou, Correlation and prediction of dense fluid transport coefficients, Fluid Phase Equilib. 15 (1994) 189–201, https://doi.org/10.1016/0378-3812(92)87021-E.
[54] J.F. Eykman, Recherches réfractométriques (suite), Recl. Des Trav. Chim. Des Pays-Bas. 14 (1895) 185–202, https://doi.org/10.1002/recl.18950140702.
[55] J.J. Cano-Gómez, G.A. Iglesias-Silva, V. Rico-Ramírez, M. Ramos-Estrada, K.R. Hall, A new correlation for the prediction of refractive index and liquid densities of 1-alcohols, Fluid Phase Equilib. 387 (2015) 117–120, https://doi.org/10.1016/j.fluid.2014.12.015.
[56] J.J. Cano-Gómez, G.A. Iglesias-Silva, M. Ramos-Estrada, Correlations for the prediction of the density and viscosity of 1-alcohols at high pressures, Fluid Phase Equilib. 404 (2015) 109–117, https://doi.org/10.1016/j.fluid.2015.06.042.
[57] H. Liu, C.M. Silva, E.A. Macedo, Generalised free-volume theory for transport properties and new trends about the relationship between free volume and equations of state, Fluid Phase Equilib. 202 (2002) 89–107, https://doi.org/10.1016/S0378-3812(02)00083-3.
[58] H. Liu, C.M. Silva, E.A. Macedo, Unified approach to the self-diffusion coefficients of dense fluids over wide ranges of temperature and pressure - hard-sphere, square-well, Lennard-Jones and real substances, Chem. Eng. Sci. 53 (1998) 2403–2422, https://doi.org/10.1016/S0009-2509(98)00036-0.
[59] C.M. Silva, H. Liu, E.A. Macedo, Models for self-diffusion coefficients of dense fluids, including hydrogen-bonding substances, Chem. Eng. Sci. 53 (1998) 2423–2429, https://doi.org/10.1016/S0009-2509(98)00037-2.
[60] R.V. Vaz, J.R.B. Gomes, C.M. Silva, Molecular dynamics simulation of diffusion coefficients and structural properties of ketones in supercritical CO_2 at infinite dilution, J. Supercrit. Fluids 107 (2016) 630–638, https://doi.org/10.1016/J.SUPFLU.2015.07.025.
[61] J. Leite, A.L. Magalhães, A.A. Valente, C.M. Silva, Measurement and modelling of tracer diffusivities of gallic acid in liquid ethanol and in supercritical CO_2 modified with ethanol, J. Supercrit. Fluids 131 (2018) 130–139, https://doi.org/10.1016/j.supflu.2017.09.004.
[62] R.C. Reid, J.M. Prausnitz, B.E. Poling, The Properties of Gases and Liquids, Fourth ed., McGraw-Hill International Editions, New York, 1987.
[63] C.L. Yaws, Thermophysical Properties of Chemicals and Hydrocarbons, William Andrew Inc., New York, 2008.
[64] J.H. Dymond, M.J. Assael, Modified Hard-Spheres Scheme, in: J. Millat, J.H. Dymond, C.A. Nieto de Castro (Eds.), Transport Properties of Fluids - Their Correlation, Cambridge University Press, Cambridge, Prediction and Estimation, 1996, pp. 226–249.